ISSN (Print) 1226-1750
ISSN (Online) 2233-6656
Journal of Magnetics 20(4), 432-438 (2015) http://dx.doi.org/10.4283/JMAG.2015.20.4.432

Analytical and Experimental Study for Electromagnetic Performances of a Tubular Linear Machine with Axially Magnetized Single-sided Permanent Magnets

Kyung-Hun Shin[1], Kyoung-Hun Jeong[1], Jang-Young Choi[1]*, Keyyong Hong[2], and Kyong-Hwan Kim[2]

[1]*Department of Electrical Engineering, Chungnam National University, Daejeon 34134, Korea*
[2]*Offshore Plant Research Division, Korea Research Institute of Ships and Ocean Engineering, Daejeon 34103, Korea*

(Received 1 September 2015, Received in final form 10 November 2015, Accepted 13 November 2015)

This paper presents an electromagnetic analysis of a tubular linear machine with axially magnetized permanent magnets using improved analytical techniques. Based on the magnetic vector potential and a two-dimensional polar-coordinate system, the magnetic field and armature reaction field can be derived. Using these, equivalent circuit parameters, such as the electromotive force and inductance, can be obtained analytically. Finally, the generating characteristics are derived with the equivalent circuit method. In this study, the finite element method was employed to provide a comparative evaluation, and experiments were conducted to validate the results of the analytical analysis.

Keywords : tubular linear machine, permanent magnet, armature reaction field, analytical solution

1. Introduction

Recently, tubular linear machines (TLMs) have been employed in an increasingly wide range of industries, ranging from transportation, manufacturing, and office automation to material processing, healthcare, and electrical power generation. TLMs are popular because they offer high force density and bandwidth, and because of the absence of end windings and zero net attractive force [1]. Linear electromagnetic actuators are able to provide thrust force directly to the load without mechanical gears and transmission. Consequently, they offer significant advantages over rotary machines in terms of simplicity and efficiency [2]. Using high-energy permanent magnets (PMs) rather than windings is beneficial. The former have a simple rotor design without field windings, slip rings, and exciter generators, and this allows them to avoid heat dissipation in the rotor to provide higher overall efficiency. This improves the performance of PM linear machine drives, which can be used as high-performance machine solutions [3, 4]. An axially magnetized permanent magnet (AMPM) topology can be produced at low costs, because its PMs are easily magnetized [5]. However, in slotted machines, detent force is produced as a result of the interaction between PMs and the slotted core, and this can affect the control accuracy [6]. Therefore, an AMPM topology is suitable for TLMs with a slotless winding structure, an example of which is illustrated in Fig. 1.

However, the magnetization of a PM mover composed of AMPMs and iron poles cannot be modeled homogeneously [5], resulting in complicated boundary conditions in the z-direction [7]. These boundary conditions make it difficult to approach analytically. Therefore, in this paper, we adopt a method based on the assumption that iron poles are identical to radially magnetized PMs [8]. Using the results from magneto-static calculations based on the finite element method (FEM), the boundary

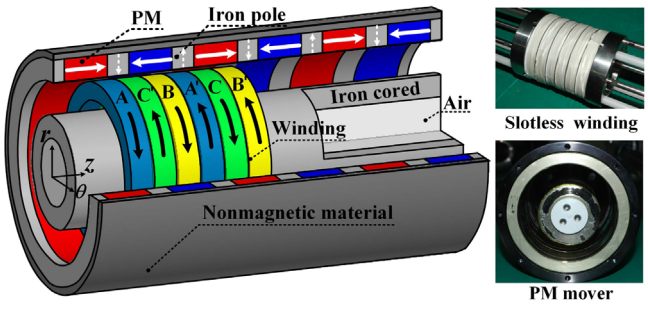

Fig. 1. (Color online) Structure of a tubular linear synchronous machine with single-sided axially magnetized permanent magnets.

*Corresponding author: Tel: +82-42-821-7610
Fax: +82-42-822-4933, e-mail: choi_jy@cnu.ac.kr

conditions for the magnetic field can be simplified. Furthermore, Carter's coefficient is applied to the model for a TLM with an AMPM topology and iron poles. Based on improved analytic techniques, the magnetic field resulting from the PMs and the armature reaction field from the coils can be derived, and equivalent circuit parameters and the generating characteristics can, in turn, be calculated. The validity of the proposed analytical method was verified experimentally, and it was evaluated by comparing its results with the results of the FEM.

2. Analytical Magnetic-field Calculations

2.1. Analytical model and assumptions

Figure 2 shows the analytical model for TLMs with AMPMs. The PMs and iron poles on the outer mover are arranged to form a magnetic path through the air gap. Here, R_{om} and R_{im} respectively denote the outer and inner radii of the outer mover topology; R_{ow} and R_{iw} respectively denote the outer and inner radii of the outer coreless-winding topology; and R_{oc} and R_{ic} respectively denote the outer and inner radii of the inner-core topology. With the exception of the iron core, the permeability of all materials used in this model is assumed to be equal to that of air (μ_0).

2.2. Using virtual magnetization to calculate the magnetic field resulting from the PM

To calculate the magnetic field produced by the PMs, the proposed analytical model considers three regions, as shown in Fig. 2: nonmagnetic material (**I**), the outer mover topology (**II**), and the air gap and coreless winding (**III**).

Based on the analytical method introduced in [8], the magnetic flux of the iron pole can be assumed to have a magnetization component in the vertical direction coming from PMs with a magnetization component in the

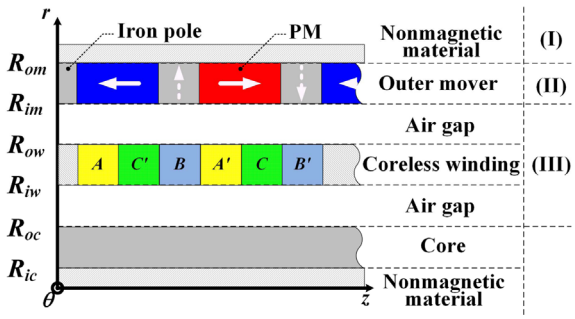

Fig. 2. (Color online) Simplified analytical model for predicting the magnetic field resulting from a PM.

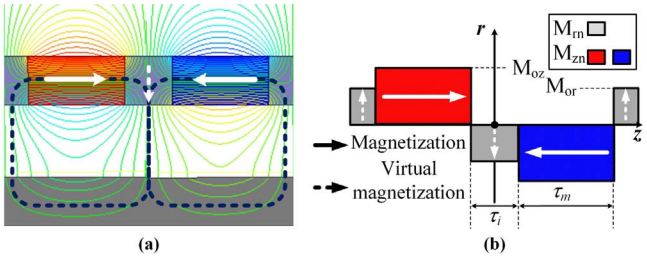

Fig. 3. (Color online) (a) Flux-line distributions and (b) magnetization model for the outer magnet topology.

horizontal direction, as shown in Fig. 3(a).

Figure 3(b) shows the Fourier series expression for the magnetization of the outer magnet topology, represented as follows:

$$\mathbf{M^{II}} = \sum_{n=-\infty,odd}^{\infty}\left[\left(\frac{c_1}{r}+c_2 r\right)M_{rn}^{II}\mathbf{i_r}+M_{zn}^{II}\mathbf{i_z}\right]e^{-jk_n z}, \quad (1)$$

where $c_1 = R_{om}R_{im}/(R_{om}+R_{im})$, $c_2 = 1/(R_{im}+R_{om})$, $k_n = nt/p$, and t denotes the pole pitch. Coefficients c_1 and c_2 in Equation (1) are used to represent M_{rn}^{II} to a function of r [9], and n denotes the n^{th}-order space harmonics.

In the analytical model, the flux density **B** in the magnets can be expressed in terms of the field intensity **H** and magnetization **M** as

$$\mathbf{B} = \mu_0(\mathbf{H}+\mathbf{M}). \quad (2)$$

Because there is no free current in the PM region, $\nabla \times \mathbf{H} = 0$. Therefore, $\nabla \times \mathbf{B} = \mu_o \nabla \times \mathbf{M}$. The magnetic vector potential **A** is defined as $\nabla \times \mathbf{A} = \mathbf{B}$. Because of the geometry of the cylindrical machine, the magnetic vector potential has only A_{qn}, which is independent [10]. In non-conducting regions, the magnetic vector potential is assumed to have a Coulomb gauge dependence, and it satisfies Poisson's and Laplace's equations, stated respectively as follows:

$$\nabla^2\mathbf{A^{I,III}} = 0,$$
$$\nabla^2\mathbf{A^{II}} = -\mu_0(\nabla\times\mathbf{M^{II}}). \quad (3)$$

By solving Equation (3), the following equation can be derived:

$$\frac{\partial^2 A_{\theta n}^{I,III}}{\partial r^2}+\frac{1}{r}\frac{\partial A_{\theta n}^{I,III}}{\partial r}-\left(k_n^{\,2}+\frac{m_k^{\,2}}{r^2}\right)A_{\theta n}^{I,III}=0,$$
$$\frac{\partial^2 A_{\theta n}^{II}}{\partial r^2}+\frac{1}{r}\frac{\partial A_{\theta n}^{II}}{\partial r}-\left(k_n^{\,2}+\frac{m_k^{\,2}}{r^2}\right)A_{\theta n}^{II}=jk_n\mu_0\left(\frac{c_1}{r}+c_2 r\right)M_{rn}^{II}. \quad (4)$$

Moreover, Equation (5) can be solved when the m_k is simplified to 1:

$$A_{\theta n}^{I,III} = A_n^{I,III} I_1(k_n r) + B_n^{I,III} K_1(k_n r),$$
$$A_{\theta n}^{II} = A_n^{II} I_1(k_n r) + B_n^{II} K_1(k_n r) - \frac{j\mu_0}{k_n}\left(\frac{c_1}{r} + c_2 r\right) M_{rn}^{II}. \quad (5)$$

Finally, using the definition of the magnetic vector potential, the normal magnetic flux density ($\mathbf{B_r^{PM}}$) and the tangential magnetic flux density ($\mathbf{B_z^{PM}}$) from the PM can be derived as follows:

$$\mathbf{B}_{\mathbf{rn}}^{\mathbf{I,II,III}} = \sum_{n=-\infty,odd}^{\infty} jk_n A_{\theta n} e^{-jk_n z}\mathbf{i}_{\mathbf{r}},$$
$$\mathbf{B}_{\mathbf{zn}}^{\mathbf{I,II,III}} = \sum_{n=-\infty,odd}^{\infty}\left(\frac{A_{\theta n}}{r} + \frac{\partial A_{\theta n}}{\partial r}\right) e^{-jk_n z}\mathbf{i}_{\mathbf{z}}. \quad (6)$$

The undefined coefficients $A_n^{I,II,III}$ and $B_n^{I,II,III}$ can be determined using the following boundary conditions :

(i) $\lim_{r\to\infty} \mathbf{B_r^I}(r) = 0$ and $K_1(\infty) = 0$, because of the identities of the modified Bessel functions: the second kind.
(ii) $\mathbf{B_r^I}(R_{om}) = \mathbf{B_r^{II}}(R_{om})$ and $\mathbf{B_r^{II}}(R_{im}) = \mathbf{B_r^{III}}(R_{im})$, because of the continuity of magnetic vector potentials at each boundary.
(iii) $\mathbf{B_z^I}(R_{om}) + \mu_0\mathbf{M_z} = \mathbf{B_z^{II}}(R_{om})$ and $\mathbf{B_z^{III}}(R_{im}) + \mu_0\mathbf{M_z} = \mathbf{B_z^{II}}(R_{im})$, because the equivalent current owing to Halbach magnetization exists at the upper and lower surfaces of the outer PMs.
(iv) $\mathbf{B_z^{III}}(R_{oc}) = 0$, because the permeability of the iron core is assumed to be infinite, and the tangential components of **H** are continuous at $r = R_{oc}$, owing to the absence of surface current density.

2.3. Using Cater's coefficient to calculate the armature reaction field from the coils

To obtain the armature reaction field, the proposed analytical model considers three regions, as shown in Fig. 4. Here, τ_m, τ_c, τ_{sp}, and τ_{cw} denote the PM width, coil pitch, slot pitch, and slot width, respectively. For TLMs with AMPMs, the influence of the iron pole can be accounted for by applying Carter's coefficient, K_c [11]:

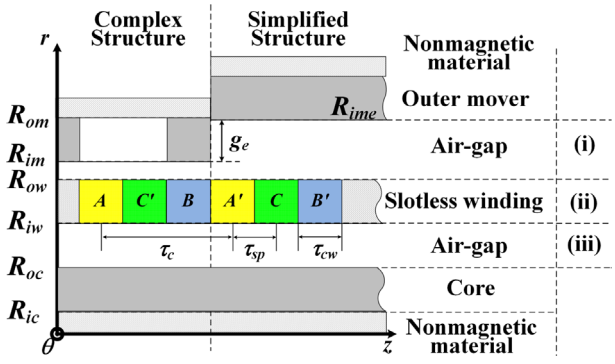

Fig. 4. (Color online) Simplified analytical model for predicting the armature reaction field.

$$K_c = \frac{\tau_{sp}}{\tau_{sp} - \gamma g}, \quad (7)$$

where g is the length of the air gap. The opening factor g is given by

$$\gamma = \frac{4}{\pi}\left(\frac{\tau_m}{2g}\tan^{-1}\left(\frac{\tau_m}{2g}\right) - \ln\sqrt{1+\left(\frac{\tau_m}{2g}\right)^2}\right). \quad (8)$$

Therefore, the effective air-gap length g_e and the equivalent outer mover radius R_{ime} are given respectively as follows:

$$g_e = g + (K_c - 1)g,$$
$$R_{ime} = R_{im} + g_e. \quad (9)$$

The Fourier series expression for the current densities of the phase are represented by

$$\mathbf{J}^{\mathbf{ii}} = \sum_{n=-\infty,odd}^{\infty}\left\{\left(\frac{c_3}{r} + c_4 r\right) J_{\theta n}\mathbf{i}_{\boldsymbol{\theta}}\right\} e^{-jk_n z}, \quad (10)$$

where $c_3 = R_{ow}R_{iw}/(R_{ow} + R_{iw})$ and $c_4 = 1/(R_{ow} + R_{iw})$. Coefficients c_3 and c_4 in Equation (10) are used to represent the current density components in a function of r. In electrical machines with three-phase winding, these windings are spaced 120 electrical degrees apart. The Fourier coefficient J_{qn} consists of $J_0 = N_{turn}i/S_c$, where N_{turn}, I, and S_c denote the number of conductors, the flowing current, and the area of the coil, respectively.

In regions (**i**) and (**iii**), $\mathbf{J} = \nabla \times \mathbf{H} = 0$ and $\mathbf{M} = 0$, owing to the absence of free current and magnetization, respectively. Likewise, in region (**ii**), $\mathbf{M} = 0$, because of the absence of magnetization. From Equation (2), the governing equations can be obtained, as mentioned above:

$$\nabla^2\mathbf{A}^{\mathbf{i,iii}} = 0,$$
$$\nabla^2\mathbf{A}^{\mathbf{ii}} = -\mu_0\mathbf{J}^{\mathbf{ii}}. \quad (11)$$

Here, the superscripts **i**, **ii**, and **iii** denote the outer air gap, coreless winding, and inner air gap regions, respectively. Equation (11) can also be solved as follows:

$$A_{\theta n}^{i,iii} = A_n^{i,iii} I_1(k_n r) + B_n^{i,iii} K_1(k_n r),$$
$$A_{\theta n}^{ii} = A_n^{ii} I_1(k_n r) + B_n^{ii} K_1(k_n r) + \frac{\mu_0}{k_n^2}\left(\frac{c_3}{r} + c_4 r\right) J_{\theta n}. \quad (12)$$

Finally, using the definition of the magnetic vector

potential, the normal magnetic flux density ($\mathbf{B}_r^{coil}$) and the tangential magnetic flux density ($\mathbf{B}_z^{coil}$) from the coil are derived as follows:

$$\mathbf{B}_r^{coil} = \sum_{n=-\infty,odd}^{\infty} jk_n A_{\theta n} e^{-jk_n z}\mathbf{i}_r,$$

$$\mathbf{B}_z^{coil} = \sum_{n=-\infty,odd}^{\infty} \left(\frac{A_{\theta n}}{r} + \frac{\partial A_{\theta n}}{\partial r}\right) e^{-jk_n z}\mathbf{i}_z. \quad (13)$$

The undefined coefficients $A_n^{i,ii,iii}$ and $B_n^{i,ii,iii}$ can be determined by using the following boundary conditions:

(i) $\mathbf{B}_z^{i}(R_{ime}) = 0$, because the influence of the iron pole can be accounted for, given that the permeability of the outer mover is assumed to be infinite, and the tangential components of **H** are continuous at $r = R_{ime}$, owing to the absence of any surface current density.

(ii) $\mathbf{B}_r^{i}(R_{ow}) = \mathbf{B}_r^{ii}(R_{ow})$ and $\mathbf{B}_r^{ii}(R_{iw}) = \mathbf{B}_r^{iii}(R_{iw})$, owing to the continuity of magnetic vector potentials at each boundary.

(iii) $\mathbf{B}_z^{i}(R_{ow}) = \mathbf{B}_z^{ii}(R_{ow})$ and $\mathbf{B}_z^{ii}(R_{iw}) = \mathbf{B}_z^{iii}(R_{iw})$, because there is no surface current at the upper and lower surface of the coreless winding regions.

(iv) $\mathbf{B}_z^{iii}(R_{oc}) = 0$, because the permeability of the iron core is assumed to be infinite, and the tangential components of **H** are continuous at $r = R_{oc}$, owing to the absence of any surface current density.

3. Electrical Parameters and Generating Characteristics

3.1. Back-EMF

The flux linkages are computed by considering the distribution of windings within the thin sheet in the each layer of the coreless winding region, with the coil pitch τ_c. When the mover is shifted along the axial direction in the (r, θ, z) coordinate system, and when the coreless windings are fixed within the (r, θ, a) coordinate system, their relationship is given by $\alpha = z + ut$, where u is the speed of the mover and t is the movement time.

Therefore, the flux linkage for each coil turn (ϕ_{pm}) can be derived as follows:

$$\begin{aligned}\phi_{pm} &= \int_0^{\tau_c}\int_0^{2\pi} \mathbf{B}_{rn}^{III} r d\theta d\alpha,\\ &= \int_0^{\tau_c}\int_0^{2\pi} jk_n\left(A_n^{III} I_1(k_n r) + B_n^{III} K_1(k_n r)\right) e^{-jk_n(\alpha-ut)} r d\theta d\alpha,\\ &= -2\pi r\left(A_n^{III} I_1(k_n r) + B_n^{III} K_1(k_n r)\right)\left(e^{-jk_n\tau_c} - 1\right) e^{jk_n ut}. \end{aligned} \quad (14)$$

The flux linkage per phase resulting from the PMs (λ_{pm}) is given by $\lambda_{pm} = N_{turn}\phi_{pm}$, where N_{turn} is the number of turns per slot. The stranded coils distributed along the radial and axial directions are denoted by r_n and n_z, respectively, as shown in Fig. 5.

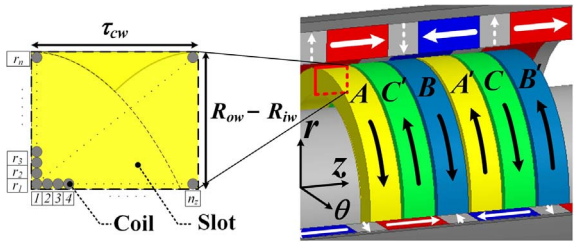

Fig. 5. (Color online) Illustration of winding for calculating electrical parameters.

Finally, the back-EMF can be calculated as follows:

$$\begin{aligned} e &= -\frac{d\lambda_{pm}}{dt}\\ &= \sum_{r_n=r_1}^{r_n}\sum_{n_z=1}^{n_z} -jk_n n_z u\left(-2\pi r\left(A_n^{III} I_1(k_n r) + B_n^{III} K_1(k_n r)\right)\left(e^{-jk_n\tau_c} - 1\right) e^{jk_n ut}\right) \end{aligned} \quad (15)$$

3.2. Inductance calculations

The flux linkage per turn resulting from the coil is given by

$$\begin{aligned}\phi_{coil} &= \int_0^{\tau_c}\int_0^{2\pi} \mathbf{B}_{rn}^{ii} r d\theta dz,\\ &= \int_0^{\tau_c}\int_0^{2\pi} jk_n\left(A_n^{ii} I_1(k_n r) + B_n^{ii} K_1(k_n r) + \frac{\mu_0}{k_n^2}\left(\frac{c_3}{r} + c_4 r\right) J_{\theta n}\right) e^{-jk_n z} r d\theta dz,\\ &= 2\pi r\left(A_n^{ii} I_1(k_n r) + B_n^{ii} K_1(k_n r) + \frac{\mu_0}{k_n^2}\left(\frac{c_3}{r} + c_4 r\right) J_{\theta n}\right)\left(e^{-jk_n\tau_c} - 1\right). \end{aligned} \quad (16)$$

The flux linkage per phase from the armature reaction (λ_{coil}) is given by $\lambda_{coil} = N_{turn}\phi_{coil}$. If the leakage inductance is ignored, the self-inductance per phase (L_{self}) can be derived as follows:

$$\begin{aligned} L_{self} &= \frac{\lambda_{coil}}{i}\\ &= \sum_{r_n=r_1}^{r_n}\sum_{n_z=1}^{n_z} 2\pi r_n n_z\left(A_n^{ii} I_1(k_n r) + B_n^{ii} K_1(k_n r) + \frac{\mu_0}{k_n^2}\left(\frac{C_1}{r} + C_2 r\right) J_{\theta n}\right)\left(e^{-jk_n\tau_c} - 1\right). \end{aligned} \quad (17)$$

In the case of a PM synchronous machine with three-phase winding where the phases are 120 electrical degrees apart, the mutual inductance (M) is expressed as

$$M = -\frac{1}{2} L_{self}. \quad (18)$$

The synchronous inductance (L_s) can be derived with the following equation:

$$\begin{aligned}\Phi_a &= L_{self} i_a + M i_b + M i_c\\ &= \frac{3}{2} L_{self} i_a\\ &= L_s i_a, \end{aligned} \quad (19)$$

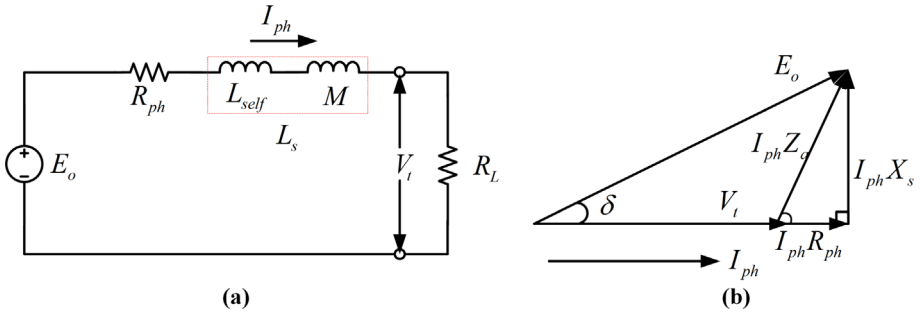

Fig. 6. (Color online) Equivalent circuit of a TLM: (a) simplified equivalent circuit, (b) vector diagram for the case when power factor is unity.

where Φ_a is the flux linkage of phase A.

3.3. Analyzing the generating characteristics

The resistance per phase (R_{ph}) can be calculated by $R_{ph} = N_{turn}\,\rho_c\,\lambda_c/A_c$, where ρ_c is the electrical resistivity of the conductor, l_c is the circumference of the coil given by $l_c = 2\pi\,(R_{ow} + R_{iw})/2$, and A_c is the cross-sectional area of the coil given by $A_c = \pi\,r_c^2$. Here, r_c is the radius of the coil.

As shown Fig. 6, the equivalent circuit for a single phase requires the following circuit parameters: no-load induced voltage (E_0), phase current (I_{ph}), synchronous inductance (L_s), resistance per phase (R_{ph}), load resistance (R_L), and terminal voltage (V_t). Using these parameters, the generating characteristics are derived using the equivalent circuit method (ECM). First, the phase current is calculated as follows:

$$I_{ph} = \frac{E_0}{\sqrt{(R_{ph}+R_L)^2 + X_s^{\,2}}}, \tag{20}$$

where X_s is the synchronous reactance given by $X_s = 2\pi f L_s$. Here, f is the frequency of the no-load induced voltage.

The terminal voltage is derived as follows:

$$V_t = E_o\sqrt{\frac{R_L^{\,2}}{(R_{ph}+R_L)^2 + X_s^{\,2}}}. \tag{21}$$

Finally, the output power (P_{out}) is determined with the following equation:

$$P_{out} = 3V_{t,rms}I_{ph,rms}, \tag{22}$$

where V_{t_rms} and I_{ph_rms} are the root-mean-square (*rms*) values for the terminal voltage and the phase current, respectively. Equation (22) represents the sum of powers for the three phases.

4. Validation and Experimental Testing

The open circuit field and the armature reaction field are the electro-magnetic phenomena caused by the outer PMs and the current flowing through the coil, as shown in Fig. 7. The specifications and design parameters are presented in Table 1. Moreover, in order to verify the performance of the proposed method, an experimental system was implemented on a double-sided TLM and load bank, as shown in Fig. 8.

Figure 9 shows a comparison of the proposed analytical results with the FEM results, along with the experimental results from measuring the back-EMF of a single phase. The proposed analytical method and the FEM were

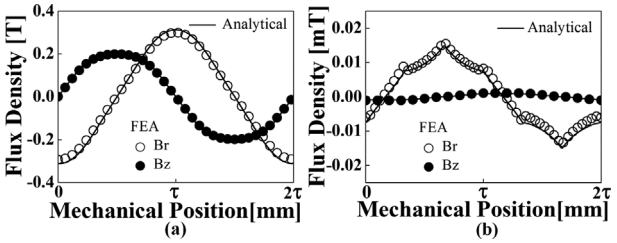

Fig. 7. Comparing the analytical results with the FEM results at the center of the coil (a) magnetic flux density from the PMs and (b) magnetic flux density from the coils.

Table 1. Specifications for the actual tubular linear machine.

Symbol	Designation	Unit	Value
R_{om}	Outer radius of the outer mover topology	mm	50
R_{im}	Inner radius of the outer mover topology	mm	40
R_{oc}	Outer radius of the inner-core topology	mm	25
R_{ic}	Inner radius of the inner-core topology	mm	15
R_{ow}	Outer radius of the coreless winding	mm	37
R_{iw}	Inner radius of the coreless winding	mm	29.5
τ	Pole pitch	mm	30
τ_{cw}	Axial length of a slot	mm	10
τ_i	Axial length of an iron pole	mm	10
τ_m	Axial length of a permanent magnet	mm	20
N_{turn}	Number of turns per slot	-	200
B_r	Remanent flux density	T	1.3
μ_0	Permeability of air	H/m	$4\pi \times 10^{-7}$
u	Maximum mover speed	m/s	0.3

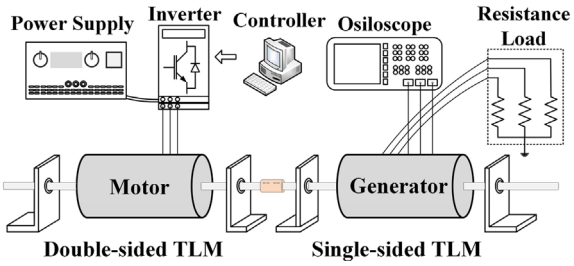

Fig. 8. (Color online) Experimental setup.

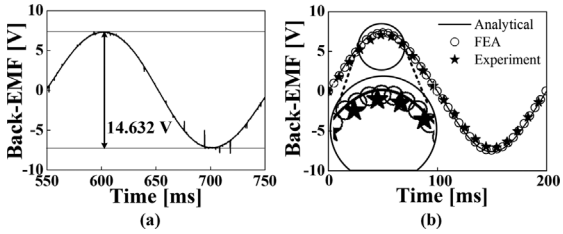

Fig. 9. (a) Experimental results from measuring the back-EMF and (b) comparing the analytical results with the FEM results in terms of the back-EMF of a single phase.

Table 2. Predictions and measurements of electrical parameters.

Symbol	Description	Unit	Value		
			Analytical	FEM	Meas.
E_0	Back-EMF	V	7.605	7.405	7.316
L_s	Inductance	mH	9.174	10.16	8.19
R_{ph}	Resistance	Ω	5.1188		6.01

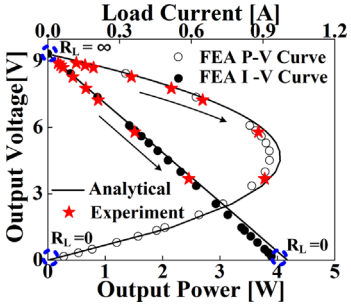

Fig. 10. (Color online) Comparing the predictions with measurements of the P-V and I-V curves according to load resistance (R_L).

evaluated under the condition of the rated speed, u. Table 2 shows the predictions and measurements for electrical parameters such as the back-EMF, inductance, and resistance. Figure 10 shows the generating characteristics at the rated mover speed. The generating characteristics were obtained according to various load resistances (R_L).

In these figures, the overall analytical results were found to agree with the FEM results and measurements. However, there were some differences when testing the method at maximum output power. These differences are the result of the manufacturing and measuring process. Nevertheless, the differences are so slight as to be negligible.

5. Conclusions

This paper offered an analysis of the electromagnetic characteristics of a TLM with AMPMs. The boundary conditions for axially magnetized machines are challenging when approached analytically, because the outer mover topologies are composed of PMs and iron poles, and these cannot be modeled homogeneously. To solve this problem, the proposed method assumes that iron poles are identical to radially magnetized PMs. This way, the armature reaction field can be derived using Carter's coefficient. These assumptions were made to simplify the (otherwise complex) analytical model.

Based on a magnetic vector potential and a two-dimensional polar-coordinate system, the governing equations for deriving the magnetic flux density from the PMs were obtained, along with the armature reaction. From these equations, equivalent circuit parameters were obtained–e.g., the electromotive force, inductance, and resistance. Further, the generating characteristics were derived by applying these parameters to the equivalent circuit method. Finally, by comparing the analytical predictions with results from the FEM, the validity of the analytical method presented in this paper was verified. These results suggest that the proposed method can be used as a convenient tool in similar studies or initial designs in order to reduce the time required for electromagnetic analysis.

Acknowledgements

This work was supported by the project "Development of the design technologies for a 10 MW class wave and offshore wind hybrid power generation system", and also supported by the Basic Science Research Program through the Ministry of Science, ICT and Future Planning, National Research Foundation of Korea under Grant 2014R1A1A1A05002745.

References

[1] B. L. J. Gysen, J. J. H. Paulides, E. A. Lomonova, and A. J. A. Vandenput, IEEE Trans. Magn. **44**, 1751 (2008).
[2] Antonino Musolino, Marco Raugi, Rocco Rizzo, and Mauro Tucci, IEEE Trans. Magn. **50**, 1 (2014).
[3] Shan Peng, W. N. Fu, and S. L. Ho, IEEE Trans. Magn. **50**, 1 (2014).

[4] Gündoğdu, Tayfun and Güven Kömürgöz, J. Magn. Magn. Mater. **324**, 2679 (2012).
[5] J. Wang, G. W. Jewell, and D. Howe, IEEE Trans. Magn. **35**, 1986 (1999).
[6] Wang, Xiuhe, Yubo Yang, and Dajin Fu, J. Magn. Magn. Mater. **267**, 80 (2003).
[7] J. Wang, D. Howe, and G. W. Jewell, IEEE Trans. Energy Conversion **19**, 289 (2004).
[8] M. G. Park, J. Y. Choi, H. J. Shin, K. S. Lee, and K. Y. Hong, IEEE Trans. Magn. **50**, 1 (2014).
[9] N. Bianchi, IEEE Ind. Appl. Conf. **1**, 21 (2000).
[10] S. M. Jang, H. W. Cho, and S. K. Choi, IEEE Trans. Magn. **43**, 2573 (2007).
[11] J. Wang and D. Howe, IEEE Trans. Magn. **41**, 2470 (2005).